Monthly Notices
of the
ROYAL ASTRONOMICAL SOCIETY

MNRAS **452,** 3679–3688 (2015) doi:10.1093/mnras/stv1590

# A test for asymptotic giant branch evolution theories: planetary nebulae in the Large Magellanic Cloud

P. Ventura,[1]★ L. Stanghellini,[2] F. Dell'Agli,[1,3] D. A. García-Hernández[4,5] and M. Di Criscienzo[1]

[1]*INAF – Osservatorio Astronomico di Roma, Via Frascati 33, I-00040, Monte Porzio Catone (RM), Italy*
[2]*National Optical Astronomy Observatory, 950 N. Cherry Avenue, Tucson, AZ 85719, USA*
[3]*Dipartimento di Fisica, Università di Roma 'La Sapienza', P.le Aldo Moro 5, I-00143, Roma, Italy*
[4]*Instituto de Astrofísica de Canarias, E-38205 La Laguna, Tenerife, Spain*
[5]*Departamento de Astrofísica, Universidad de La Laguna (ULL), E-38206 La Laguna, Tenerife, Spain*

Accepted 2015 July 13. Received 2015 July 13; in original form 2015 June 9

## ABSTRACT

We used a new generation of asymptotic giant branch (AGB) stellar models that include dust formation in the stellar winds to find the links between evolutionary models and the observed properties of a homogeneous sample of Large Magellanic Cloud (LMC) planetary nebulae (PNe). Comparison between the evolutionary yields of elements such as CNO and the corresponding observed chemical abundances is a powerful tool to shed light on evolutionary processes such as hot bottom burning (HBB) and third dredge-up (TDU). We found that the occurrence of HBB is needed to interpret the nitrogen-enriched ($\log(N/H)+12>8$) PNe. In particular, N-rich PNe with the lowest carbon content are nicely reproduced by AGB models of mass $M \geq 6\,M_{\odot}$, whose surface chemistry reflects the pure effects of HBB. PNe with $\log(N/H)+12<7.5$ correspond to ejecta of stars that have not experienced HBB, with initial mass below $\sim 3\,M_{\odot}$. Some of these stars show very large carbon abundances, owing to the many TDU episodes experienced. We found from our LMC PN sample that there is a threshold to the amount of carbon accumulated at AGB surfaces, $\log(C/H)+12<9$. Confirmation of this constraint would indicate that, after the C-star stage is reached, AGBs experience only a few thermal pulses, which suggests a rapid loss of the external mantle, probably owing to the effects of radiation pressure on carbonaceous dust particles present in the circumstellar envelope. The implications of these findings for AGB evolution theories and the need to extend the PN sample currently available are discussed.

**Key words:** stars: abundances – stars: AGB and post-AGB – stars: carbon.

## 1 INTRODUCTION

The Large Magellanic Cloud (LMC), due to its proximity ($d \sim 50$ kpc; Feast 1999) and low average reddening ($E(B-V) \sim 0.075$; Schlegel, Finkbeiner & Davis 1998), has been used successfully as a laboratory to test asymptotic giant branch (AGB) evolution. The AGB population of the LMC has been thoroughly investigated by means of dedicated photometric surveys: the Magellanic Clouds Photometric Survey (MCPS; Zaritsky et al. 2004), the Two Micron All Sky Survey (2MASS; Skrutskie et al. 2006), the Deep Near Infrared Survey of the Southern Sky (DENIS; Epchtein et al. 1994), Surveying the Agents of a Galaxy's Evolution Survey (SAGE-LMC with the *Spitzer* telescope; Meixner et al. 2006), and *HERschel* Inventory of the Agents of Galaxy Evolution (HERITAGE; Meixner et al. 2010, 2013). Additional data allowed the reconstruction of the star formation history of the LMC (Harris & Zaritsky 2009; Weisz et al. 2013) and the age–metallicity relation (AMR, Carrera et al. 2008; Piatti & Geisler 2013); these studies confirmed that the stellar populations are on average subsolar in metallicity.

Such extensive data sets, interpreted with models for AGB evolution using the metallicities of LMC stars, have enlightened and deepened our understanding of the various, still poorly known, physical mechanisms characterizing the AGB phase; namely, the third dredge-up (TDU), hot bottom burning (HBB), and the rate of mass-loss.

The TDU consists in the penetration of the convective envelope following each thermal pulse. When the bottom of the convective mantle reaches regions of the star where $3\alpha$ burning has previously

★ E-mail: paolo.ventura@oa-roma.inaf.it

occurred, carbon-rich material is transported to the surface, with the consequent increase in the surface carbon abundance. Repeated TDU episodes may lead to the formation of a carbon star, with a surface C/O above unity. The luminosity function of the carbon star population in the LMC have been extensively used to draw information on the occurrence of TDU in terms of the extent of the inward penetration of the surface mantle in the after-pulse phases. The same studies also allowed the mass-loss rate experienced by these stars to be calibrated (Groenewegen & de Jong 1993; Marigo, Girardi & Bressan 1999; Marigo, Girardi & Chiosi 2003a; Izzard et al. 2004).

HBB is activated when the temperature at the bottom of the convective envelope ($T_{\rm bce}$) reaches sufficiently high values ($T_{\rm bce} > 40$ MK) to activate proton-capture nucleosynthesis, with the consequent modification of the surface chemistry, according to the equilibria of the various reactions involved (Renzini & Voli 1981; Blöcker & Schöenberner 1991). The main effects of HBB are the depletion of the surface carbon and nitrogen enrichment. For sufficiently large temperatures (above ∼90 MK) oxygen destruction also occurs during this process.

In the last few years, stellar evolution models that include the AGB phase have improved, with the inclusion of dust production in the stellar wind in the models (Ferrarotti & Gail 2006; Ventura et al. 2012a,b, 2014b; Di Criscienzo et al. 2013; Nanni et al. 2013a,b, 2014). These studies allow a step forward in our understanding of the physics of these stars because they can be used to interpret mid-infrared data of the most obscured, dust-enshrouded objects observed in dedicated surveys such as those mentioned above. The dust surrounding evolved stars reprocesses the light emitted by the central star at mid-infrared wavelengths. The study of the dust formation process is therefore mandatory to interpret their infrared colours correctly. By treating dust within the models and then comparing the resulting yields to observed abundances for similar dust-type stars one can push the comparison between yields and observed abundances further than previously done. First, by measuring the degree of obscuration of carbon stars through IR observations, one can get a handle on the TDU efficiency, since the amount of carbon accumulated at the stellar surface, which causes obscuration, depends on the efficiency of the TDU mechanism. Secondly, the amount of silicate dust formed in oxygen-rich stars is tied to the strength of the HBB experienced.

'Dusty' AGB models were used by Zhukovska & Henning (2013) and Schneider et al. (2014) to calculate the dust production rate by AGB stars in the LMC and compare them with existing estimates based on the observations. On the basis of these models, Dell'Agli et al. (2014, 2015) accomplished a characterization of the obscured stars in the LMC in terms of age, metallicity, and mass distribution. In a recent analysis, Ventura et al. (2015) showed that LMC stars experiencing HBB evolve to well-defined regions of the two-colour infrared diagram. Spectroscopic analysis of the selected sample, and in particular measurement of the C/O ratio, allows us to determine the strength of the HBB.

In order to gain insight into the LMC AGB stellar population and to get a handle on the physical mechanisms relevant for their evolution, a good opportunity is offered by the study of the planetary nebula (PN) population (Marigo et al. 2003b, 2011; Stanghellini et al. 2009). PNe are related to the final stages of the evolution of AGB stars, their ejecta being illuminated by the remnant central star. Their chemical composition therefore depends on the relative strength of TDU and HBB experienced during previous stellar phases. The chemical composition of PNe, compared to the surface chemistry of AGB stars in their final stages, provides insight into the chemical evolution of the star throughout its life, and in particular on the mechanisms that alter its surface composition during the final stages of its evolution. Whereas the analysis of the distribution of AGB stars in the near- and mid-infrared diagnostic diagrams allows a statistical approach to the problem that is useful for shedding light on the relative duration of the various evolutionary phases, PN abundances are strong constraints on stellar surface processes and yields in the final stages of AGB stellar life. On the observational side, determination of the surface chemical composition of PNe is easier than for AGBs because the optical/near-IR spectra of such cool giants are contaminated by millions of molecular lines, and deriving the abundances of individual species requires the use of spectral synthesis techniques (e.g. García-Hernández et al. 2006, 2007a, 2009), even when taking into account circumstellar effects (Zamora et al. 2014). In addition, the more massive and extreme AGBs are heavily obscured and escape detection (and abundance studies) in the optical range (e.g. García-Hernández et al. 2007b) and/or they may display extremely complex near-IR spectra (e.g. McSaveney et al. 2007).

Against this background, we embarked on testing the results of suitable AGB stellar evolution yields (Dell'Agli et al. 2015) to the observed chemical composition of the LMC PN population. The goal of this investigation is twofold. On the one hand, we attempt a characterization in terms of the progenitor mass and initial chemistry of the LMC PN sample. On the other hand, we use the PN chemical composition to help discriminate among different AGB models and paths, and to clarify still open issues related to AGB evolution, such as the strength of HBB experienced by the different star mass models, the possibility that more massive AGB stars may eventually become carbon stars, and the maximum carbon enrichment achieved by low-mass AGB stars. We constrain our study to the well-defined LMC PN sample in this paper and will extend it to other PN populations in the future.

In Section 2, we describe the stellar evolution models. Section 3 describes the changes in surface composition due to the AGB processing. Section 4 describes the observational sample used in this paper, its limitations and uncertainties, and the comparison of PN abundances with the final chemical composition from AGB evolution. A discussion is presented in Section 5, while the conclusions and future outlook are in Section 6.

## 2 THE EVOLUTION OF AGB STARS IN THE LMC

Modelling the AGB phase demands a considerable computational effort, owing to the necessity of adopting extremely short timescales, as short as a few hours, during the thermal pulses. To date, there are still considerable differences among the results presented by the various groups in this field, which just stresses the difficulty in modelling the AGB phase.

The AGB stellar models are extremely sensitive to the input physics, primarily convection and the rate of mass-loss. In the literature, there are several reviews of AGB evolution (Herwig 2005; Karakas 2011; Karakas & Lattanzio 2014), and we do not repeat them here. In the following subsections, we will present a summary of the physical input of the AGB models used in this paper.

### 2.1 Numerical and physical input

The AGB models used here are based on the evolution of the star and on a description of dust formation in the wind.

The evolutionary sequences of central stars were calculated by means of the ATON code for stellar evolution (Mazzitelli 1989). The interested reader will find in Ventura et al. (1998) a detailed discussion of the numerical structure of the code; the latest updates are given in Ventura & D'Antona (2009). Here, we briefly recall the most relevant physical input.

The temperature gradient within regions unstable to convective motion was determined by means of the Full Spectrum of Turbulence (FST; Canuto & Mazzitelli 1991) description. The efficiency of the convective transport of energy is probably the most important and relevant uncertainty affecting the results of AGB modelling (Ventura & D'Antona 2005).

Mass-loss during the AGB for O-rich phases was modelled according to Blöcker (1995). For carbon stars, we used the calibration of $\dot{M}$, based on hydrodynamical models of C-star winds, by Wachter et al. (2002, 2008).

In the low-temperature regime (below $10^4$ K) we calculated molecular opacities by means of the AESOPUS tool, developed by Marigo & Aringer (2009). The advantage of this approach is that the opacities are suitably constructed to follow the changes in the chemical composition of the envelope driven by TDU and HBB, with the possibility of accounting for changes in the individual abundances of carbon, nitrogen, and oxygen. Following this approach is crucial for the description of the carbon-rich phase because the increase in the molecular opacities occurring when the C/O ratio approaches (and overcomes) unity favours a considerable expansion of the surface layers of the star, with the consequent enhancement of the rate at which mass-loss occurs (Ventura & Marigo 2010).

The dust formation process is described in Dell'Agli et al. (2015). To span the range of metallicities of stars in the LMC (Harris & Zaritsky 2009), we used three sets of models with metallicity $Z = 10^{-3}$, $4 \times 10^{-3}$, and $8 \times 10^{-3}$.

Each model was evolved starting from the pre-main sequence phase until when almost all the external envelope was lost; prosecuting the computations until the beginning of the PN phase would demand a much greater computational effort, with no significant improvement to the results needed in this context.

### 2.2 Physical properties of AGB evolution models

The models presented here, including the discussion of the evolutionary sequences, are extensively illustrated in Ventura et al. (2014a) ($Z = 4 \times 10^{-3}$), Ventura et al. (2013) ($Z = 1$, $8 \times 10^{-3}$, initial mass above 3 $M_\odot$), and Ventura et al. (2014b) (low-mass models of metallicity $Z = 1$, $8 \times 10^{-3}$ and initial mass below 3 $M_\odot$). Here, we review the relevant aspects for this paper regarding these models.

High-mass stellar models evolve to more massive AGB stellar cores, independently of the progenitor metallicity. These massive cores correspond to a higher stellar luminosity, hence, given our mass-loss prescription, to a higher rate of mass-loss. Stars with initial masses in the range 1.25 $M_\odot \leq M_i \leq 3$ $M_\odot$ reach the C-star stage after a series of thermal pulses, each associated with a TDU episode, that gradually increases the surface stellar carbon. These limits are slightly dependent on metallicity: the lower limit to reach the C-star stage is 1 $M_\odot$ for $Z = 1, 4 \times 10^{-3}$, whereas it is 1.25 $M_\odot$ for $Z = 8 \times 10^{-3}$; the upper limit in the initial mass to enter the C-star phase is 3 $M_\odot$ for $Z = 4$, $8 \times 10^{-3}$, whereas it is 2.5 $M_\odot$ for $Z = 10^{-3}$.

After reaching a surface abundance ratio of C/O > 1, the surface molecular opacity increases (Marigo 2002; Ventura & Marigo 2009, 2010), thereby triggering expansion (and cooling) of the external regions. As a consequence, the rate of envelope mass-loss is enhanced when C/O becomes greater than unity.

A clear separation distinguishes models with initial mass below ~3 $M_\odot$ from their higher mass counterparts, which experience HBB. Stars that go through HBB will never become carbon stars, because their surface carbon is rapidly destroyed by proton-capture nucleosynthesis occurring at the base of the convective envelope.

The trend with mass in the high-mass domain (M>3 $M_\odot$) is straightforward: the higher the initial stellar mass, the higher is the temperature $T_{\rm bce}$ at which HBB occurs, the steeper the core mass versus luminosity relationship. These high-mass models lose the convective envelope very rapidly and thus experience a limited number of thermal pulses (see table 1 in Ventura et al. 2013), which prevents the possibility of any contamination of the surface chemistry by TDU.

A word of caution is needed regarding the dependence of models on physical input, particularly on convection and mass-loss rate. Models calculated with a less efficient treatment of convection than used here, such as the traditional mixing length (ML) scheme, experience weaker HBB, thus evolving at lower luminosities and losing their envelopes at a lower rate. If the ML scheme were applied, the number of thermal pulses experienced by massive AGB models would be higher than the number of pulses suffered by low-stellar mass models. As a result, massive stars would evolve as carbon stars in the very final AGB phases. An exhaustive discussion of this argument can be found in the detailed analysis by Ventura & D'Antona (2005) and in the more recent investigations by Doherty et al. (2014a,b).

## 3 CHANGE IN THE SURFACE CHEMISTRY OF AGB STARS

The variation of the surface chemical composition of the AGB models in this paper, in terms of the surface mass fractions of the CNO elements, is shown in Figs 1, 2, and 3, respectively for $Z = 10^{-3}$, $Z = 4 \times 10^{-3}$, and $Z = 8 \times 10^{-3}$. The abscissae give total stellar mass. This choice allows us to show the sequences of the different masses in the same plane, despite the difference in the evolutionary times. The initial mass of each model can be deduced from the abscissa in the starting point of each track.

### 3.1 Low-mass AGB stars: the effect of TDU

The variation of the surface carbon, shown in the left-hand panels of Figs 1, 2, and 3, reflects the relative contributions from TDU and HBB in modifying the surface chemical composition. In low-mass stars ($M < 3$ $M_\odot$), TDU is the only active mechanism; thus, the surface carbon increases during AGB evolution. For all the metallicities investigated, the largest abundances of carbon, $X(C) \sim 10^{-2}$, are reached by models with mass $M \sim 2$–2.5 $M_\odot$. The overall surface carbon abundance increases by a factor of ~10 for $Z = 8 \times 10^{-3}$, and by two orders of magnitude for $Z = 10^{-3}$. Models with mass below ~2 $M_\odot$ experience a smaller number of thermal pulses than the high-mass ones; hence, their final carbon abundance is smaller. Note that the final carbon mass fraction for stars experiencing TDU is practically independent of the initial abundance; rather, it is essentially determined by the extent of the inward penetration of the convective envelope into regions previously touched by $3\alpha$ burning during each TDU episode.

Stars of initial mass below ~1.25 $M_\odot$ (but see discussion in Section 2.2 on the sensitivity of this limit to the metallicity) do

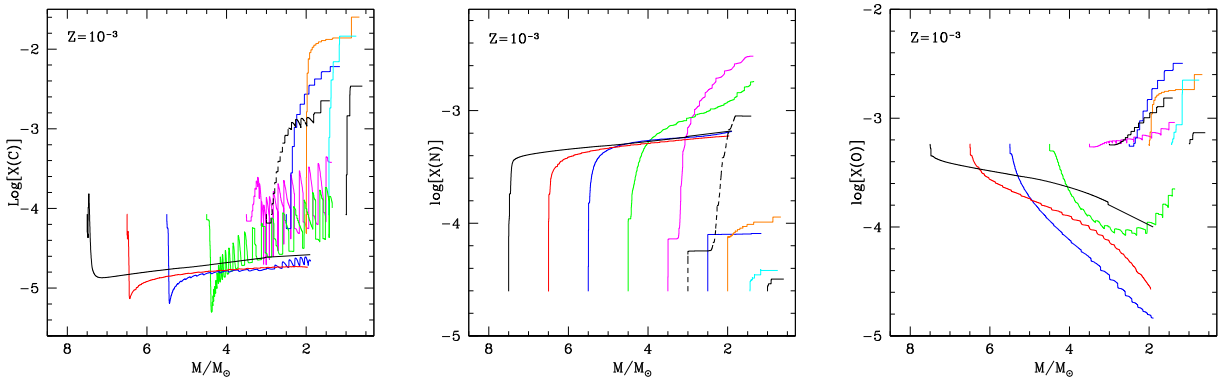


**Figure 1.** The evolution of the surface mass fraction of carbon (left), nitrogen (middle), and oxygen (right) during the AGB phase of models of initial mass in the range 1 $M_{\odot} \leq M \leq 7.5$ $M_{\odot}$ and metallicity $Z = 10^{-3}$. Along the abscissa we report the total mass of the star (decreasing during the evolution). For clarity, we show only the evolution of models of initial mass 1, 1.5, 2, 2.5, 3, 3.5, 4.5, 5.5, 6.5, and 7.5 $M_{\odot}$.

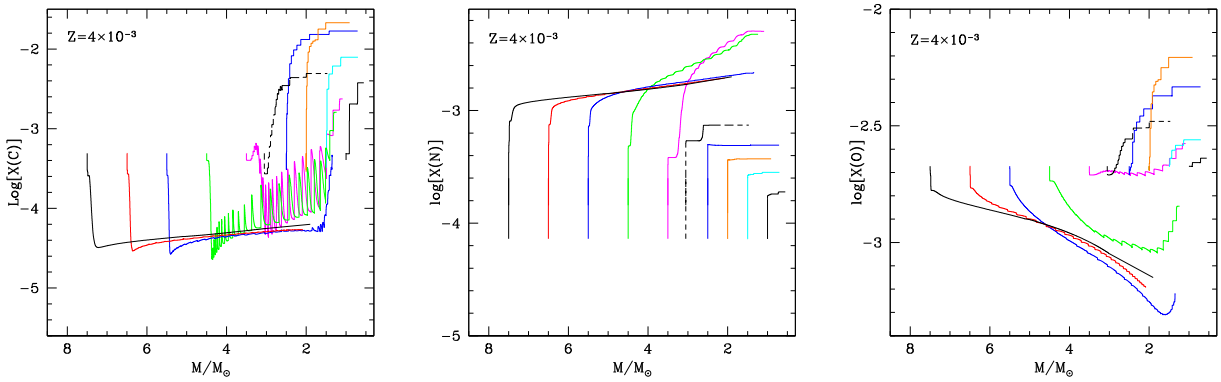


**Figure 2.** The same as in Fig. 1, but referred to AGB models of metallicity $Z = 4 \times 10^{-3}$.

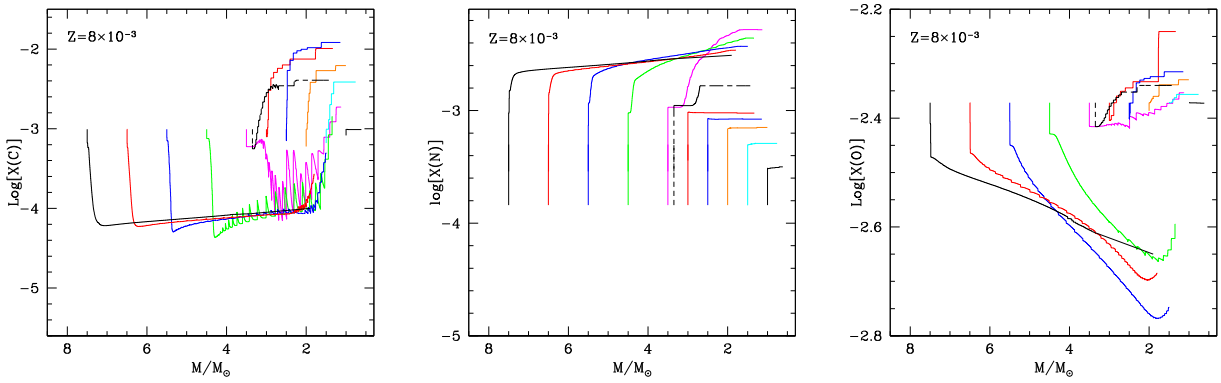


**Figure 3.** The same as in Fig. 1, but referred to AGB models of metallicity $Z = 8 \times 10^{-3}$.

not reach the final carbon star phase because they lose the external mantle after a few thermal pulses, thus experiencing only a limited number of TDU episodes. In fact, the surface chemistry of these stars is changed only by the first dredge-up, which occurs while ascending the red giant branch.

The surface oxygen also increases in low-mass AGBs (see right-hand panels of Figs 1, 2, and 3) because, during TDU, the base of the surface convection reaches layers where some production of oxygen has occurred. The percentage variation in the surface oxygen is smaller (by a factor of ∼2–3) with respect to carbon. The final oxygen surface abundance is fairly independent of the initial stellar abundance.

Unlike carbon, the surface nitrogen is not expected to undergo significant changes in low-mass AGB stars, which renders their final nitrogen abundances sensitive to the assumed initial relative abundances and to the metallicity of the star.

### 3.2 Massive AGB stars: the signature of HBB

During the AGB evolution of the higher mass stars, those that undergo HBB, the variation of the surface chemical composition depends on the strength of the HBB experienced. The effects of HBB can be seen in the sudden decrease (by a factor of ∼20) of surface carbon, occurring in the initial phases of AGB evolution for

$M \geq 4$ M$_\odot$ (see left-hand panels of Figs 1, 2, and 3). The depletion of surface carbon occurs in conjunction with the increase in nitrogen abundance (see middle panels of the figures). The final abundances of C and N depend on whether the models suffer TDU in the final evolutionary phases.

Models with mass near the upper limit of AGB evolution ($M \sim 6$–8 M$_\odot$) are expected to experience only a small number of weak thermal pulses. The chemistry of these models is not contaminated by TDU, so their final abundances will reflect the pure effects of HBB. Consequently, they will end their AGB history with a carbon abundance a factor ∼10 lower than the initial abundance. Nitrogen will be greatly enhanced (by ∼20–30) owing to the combined effects of HBB and of the first dredge-up. The final abundances of carbon and nitrogen in these stars will be determined by the equilibria of proton-capture nucleosynthesis and will therefore scale with the initial overall C+N+O content of the star.

Models of mass 4 M$_\odot \leq M \leq 6$ M$_\odot$ undergo a more complex evolution, because the initial contamination by HBB is followed by surface carbon enrichment, caused by TDU. This can be seen in the left-hand panels of Figs 1, 2, and 3, where the surface carbon undergoes a series of ups and downs, the signature of the combined effects of TDU and HBB. In the very final AGB phases the mass of the envelope falls below the threshold for HBB: the surface carbon is determined solely by TDU so that it gradually increases until the end of the AGB evolutionary phase. The final carbon abundance depends on the number of TDU episodes experienced in the very final phases, when HBB is switched off. The present computations indicate that the final carbon in the star is higher the closer its initial mass is to the lower limit to activate HBB (i.e. to ∼3.5–4 M$_\odot$). Nitrogen increases compared to its initial value, even more so than in the most massive models, owing to the bounty of carbon available both originally and from subsequent dredge-ups from the ashes of helium burning.

### 3.3 The minimum threshold mass to activate HBB

Models of mass close to the threshold mass for HBB activation, $M \sim 3$ M$_\odot$, are shown with dashed lines in Figs 1, 2, and 3; they exhibit an interesting and specific behaviour. These stars experience HBB until the repeated TDU episodes lead to the formation of a carbon star; when the C-star stage is reached HBB is extinguished, owing to the cooling of the external regions, favoured by the increase in the molecular opacities (Marigo 2007; Ventura & Marigo 2009). Note that this behaviour is found only when the low-temperature, molecular opacities for C-rich gas are used (Marigo 2002); in models using opacities calculated by neglecting carbon enhancement, HBB remains efficient until the whole envelope is lost.

The final chemistry of these stars will be somewhat intermediate between low-mass AGB stars and more massive stars experiencing full HBB: the surface N will be slightly enhanced compared to the original abundance, whereas their surface carbon will be much higher than at the beginning of their evolution.

### 3.4 The puzzling behaviour of oxygen

Oxygen deserves separate discussion in this context. As shown in the right-hand panels of Figs 1, 2, and 3, the surface oxygen decreases in all models experiencing HBB, the signature of the activation of CNO cycling. Whereas the CN cycle is efficiently activated in all cases, because it requires temperatures of the order of ∼40 MK, full CNO burning, with the destruction of the surface oxygen, requires temperatures $T \sim 90$ MK, which renders the results extremely sensitive to metallicity. Because low-$Z$ models experience more efficient HBB (Ventura et al. 2013), the depletion of the surface oxygen with respect to the original content is much higher in the $Z = 10^{-3}$ models ($\delta\log[X(\mathrm{O})] \sim 0.7$–1.5), compared to $Z = 4 \times 10^{-3}$ ($\delta\log[X(\mathrm{O})] \sim 0.5$–0.8) and $Z = 8 \times 10^{-3}$ ($\delta\log[X(\mathrm{O})] \sim 0.2$–0.3).

The trend of oxygen abundances with mass is not trivial: the stars showing the most extreme chemistry are those with mass ∼5–6 M$_\odot$, which end their evolution with less oxygen compared to their higher mass counterparts. The reason for this is that models of higher mass lose the convective envelope very rapidly, before a very advanced nucleosynthesis has occurred. This effect, as discussed in details in Ventura et al. (2013), is a consequence of the use of the FST model for convection and of the Blöcker (1995) treatment of mass-loss.

Although the evolutionary sequences used in the present investigation are interrupted before the total consumption of the external mantle, the computations are extended to a sufficiently advanced stage during the AGB evolution that the final surface chemical composition of the models can be directly compared with the observed chemical abundances of PNe. Low-mass AGBs suffer a strong mass-loss after becoming carbon stars, owing to the effects of radiation pressure on solid carbon grains formed in the wind of the star. The loss of the envelope becomes faster and faster as more carbon is accumulated to the surface layers. In all the low-mass models discussed here the calculations reach phases when the loss of the envelope became so fast that the possibility that additional TDU episodes modify the surface chemical composition can be disregarded. On the side of massive AGBs, the nuclear activity at the base of the envelope is progressively extinguished by the loss of the external mantle; this is due to the general cooling of the external regions close to the bottom of the envelope. The computations of models in this range of masses were extended in all cases until the HBB was almost completely extinguished. Had we followed the evolution until the full ejection of the envelope, we would find a slightly higher nitrogen content and a smaller oxygen abundance; however, the differences would be significantly smaller than the errors associated with the observations, presented in the next section.

## 4 PNe IN THE LMC

### 4.1 The LMC PN data base

In order to compare data and models we have used a homogeneous sample of LMC PNe whose abundances have been collected over the years based on ground and space data sets. The most important element for these comparisons, carbon, has been observed directly with STIS/*HST* in 22 PNe (Stanghellini, Shaw & Gilmore 2005). Another 17 PNe have reliable carbon abundances available in the literature (Leisy & Dennefeld 2006); upper limits to carbon for four additional PNe, and uncertain carbon determination for three PNe, are also given in the latter reference, which includes other critical elemental abundances such as helium, nitrogen, and oxygen.

In Table 1, we give the data base used in this study. Column (1) gives the most used PN name. Column (2) gives the published morphological class. Columns (3) through (5) give, respectively, the gas-phase abundances of C, N, and O (by number) of the PNe, in the usual format $\log(X/\mathrm{H})+12$. Finally, Column (6) gives, where available, the dust type from *Spitzer*/IRS observations (Stanghellini et al. 2007). We list in this table all LMC PNe that have reliable measured abundances for at least one of the CNO elements. All abundances in table 1 are from Leisy & Dennefeld (2006) and references therein. All abundances in Table 1 have been calculated

**Table 1.** Chemical composition (in terms of CNO content), dust features (if detected) and morphology of PNe in the LMC.

| Name | *M* | (C/H) | (N/H) | (O/H) | Dust type |
|---|---|---|---|---|---|
| MG 45 | E | – | 8.41 | 8.27 | – |
| SMP 01 | R | 8.40 | – | 8.34 | – |
| SMP 02 | R | – | 6.95 | 8.03 | – |
| SMP 03 | R | – | 7.03 | 7.75 | – |
| SMP 04 | E | 8.66[a] | 7.93 | 8.61 | F |
| SMP 05 | E | – | 6.34 | 8.00 | – |
| SMP 08 | R | – | 8.00 | 8.16 | – |
| SMP 09 | BC | 8.43[a] | – | – | C-rich |
| SMP 10 | P | 7.35[a] | – | – | F |
| SMP 11 | B | – | 7.10 | 7.18 | – |
| SMP 13 | BC | 7.92 | – | 8.39 | – |
| SMP 16 | B | 7.33[a] | 8.65 | 8.32 | F |
| SMP 18 | BC[b] | 8.37[a] | – | – | F |
| SMP 19 | BC | 8.46[a] | – | – | C-rich |
| SMP 21 | Q | 7.34 | 8.37 | 7.86 | O-rich |
| SMP 25 | R | 8.29[a] | 7.26 | 8.17 | C-rich |
| SMP 27 | Q | 7.84[a] | 7.10 | 8.31 | F |
| SMP 28 | P | 8.01 | – | – | – |
| SMP 29 | B | 7.49 | 8.79 | 8.05 | – |
| SMP 30 | B[b] | 7.75[a] | 8.55 | 8.24 | – |
| SMP 31 | R[b] | – | 7.03 | 7.29 | – |
| SMP 32 | R | – | 7.73 | 8.39 | – |
| SMP 33 | BC | – | 7.84 | 8.91 | – |
| SMP 34 | E | 8.13[a] | – | – | F |
| SMP 40 | ES | – | 8.14 | 8.56 | – |
| SMP 45 | B[b] | 7.58[a] | – | – | F |
| SMP 46 | BC | 8.76[a] | – | – | C-rich |
| SMP 47 | E | 8.56 | 8.69 | 8.25 | – |
| SMP 48 | E | 8.40[a] | – | 8.24 | C-rich |
| SMP 49 | R | – | 7.60 | 8.33 | – |
| SMP 53 | BC | <6.70 | 7.72 | 8.23 | – |
| SMP 54 | B | <8.14 | – | – | – |
| SMP 55 | R | – | 7.27 | 8.40 | – |
| SMP 59 | B | 7.16[a] | 8.49 | 8.52 | – |
| SMP 62 | BC | 7.27 | – | – | – |
| SMP 63 | E | 8.80 | – | 8.39 | – |
| SMP 66 | E | 8.51 | 7.61 | 8.31 | F |
| SMP 67 | B | <7.66 | 8.00 | 8.50 | – |
| SMP 68 | E | – | – | 8.94 | – |
| SMP 69 | B | <8.32 | 8.61 | 8.63 | – |
| SMP 71 | E | 8.90[a] | 8.03 | 8.63 | C-rich |
| SMP 72 | B | 8.21[a] | – | – | F |
| SMP 73 | BC | 8.78 | – | 8.66 | – |
| SMP 75 | R | – | 7.44 | 8.29 | – |
| SMP 77 | E | 9.12 | – | 8.27 | – |
| SMP 78 | BC | 8.51 | – | – | – |
| SMP 79 | BC | 8.67[a] | 8.02 | 8.34 | C-rich |
| SMP 80 | R | 7.51[a] | 7.39 | 8.34 | F |
| SMP 81 | R[b] | 7.16[a] | 7.12 | 8.25 | O-rich |
| SMP 82 | E | – | 8.59 | 8.16 | – |
| SMP 83 | B | 7.49 | – | – | – |
| SMP 84 | E | – | 7.43 | 8.15 | – |
| SMP 85 | R | 8.74 | 7.26 | 8.00 | – |
| SMP 87 | BC | – | 8.74 | 8.23 | – |
| SMP 88 | E | <8.84 | 7.79 | 7.91 | – |
| SMP 89 | BC[b] | – | – | – | – |
| SMP 91 | B | – | 8.48 | 8.27 | – |
| SMP 92 | BC | 8.21 | 7.77 | 8.62 | – |
| SMP 93 | B | 7.62[a] | 8.69 | 8.58 | – |
| SMP 95 | BC | 8.82[a] | – | – | F |
| SMP 96 | BC | – | 8.32 | 8.04 | – |
| SMP 97 | R | 8.50 | – | 8.50 | F |
| SMP 98 | R | – | – | 8.57 | – |
| SMP 99 | BC | 8.69 | 8.15 | 8.56 | C-rich |
| SMP 100 | BC[b] | 8.55 | 7.61 | 8.36 | C-rich |
| SMP 101 | BC[b] | – | – | – | – |
| SMP 102 | BC | 8.65[a] | – | 8.28 | F |

*Notes.* [a]Carbon abundance from Stanghellini et al. (2005). [b]Uncertain morphology.

with the direct method, i.e. through the calculation of electron temperature and density, and with unobserved ion emission accounted for via the ionization correction factor (ICF) method (Kingsburgh & Barlow 1994). Note that the flux and reddening correction uncertainties for these samples are minimal when compared to the uncertainties produced by the ICF method. Most PNe in which carbon has been detected are in such an excitation range that the observation of $C^{+}$, $C^{2+}$, and $C^{3+}$ directly delivers the total carbon abundance. The derived uncertainties in carbon abundances are thus small, with both Stanghellini et al. (2005) and Leisy & Dennefeld (2006) indicating uncertainties <0.1 dex in 12+log(C/H). Uncertainties in the other elements are 0.01 dex for helium, 0.1 dex in oxygen and neon, and 0.15–0.2 dex in nitrogen abundances (Leisy & Dennefeld 2006). For the three unreliable abundances mentioned above, the uncertainty can be up to 0.3–0.5 dex.

Nebular morphology is available for most of the PNe listed in the table. They are taken directly from Stanghellini et al. (2000) and Shaw et al. (2001, 2006). Here, we list only the main shapes, i.e. round (R), elliptical (E), bipolar or quadrupolar (B or Q), bipolar core (BC), and point-symmetric (P). In some cases the morphology is uncertain, as noted in the table.

Another physical characteristic that we need for this study is the dust content of the PNe. Stanghellini et al. (2007) have observed a sizeable sample (25) of LMC PNe with *Spitzer*/IRS spectroscopy, finding different dust compositions (dust types) in their circumstellar envelopes. About half of the total sample shows carbon-rich dust features (nine C-rich PNe) or featureless spectra (14 F PNe, dust-free and quite evolved PNe dominated by nebular emission lines), while a small minority (two O-rich PNe) show oxygen-rich dust features.

It is worth noting that LMC PN studies in such chemical detail, i.e. whose auroral lines have been observed for electron temperature detection, are at the bright end of the PN luminosity function. Such bright PNe are believed to have progenitors in the mid-mass range, given that the very high mass progenitors evolve too fast in the post-AGB to produce PNe that are observed at high luminosity. This translates into a very mild selection against the high AGB mass progenitors, something that is taken into account when interpreting the comparison between data and models. It is also worth noting that extragalactic PNe are typically selected from [O III] λ5007 off band–on band images. This may produce a selection effect towards higher oxygen abundance/younger progenitors. In fact, at typical LMC metallicities, higher oxygen abundance seem to favour cooling through other emission lines than [O III] 5007 Å, contrary to what happens at higher metallicities (see Stanghellini et al. 2003).

### 4.2 Loci in the diagnostic diagrams

The left-hand panel of Fig. 4 shows the observed PN abundances (by number, in the usual log(*X*/H)+12 scale) in the CN plane. The

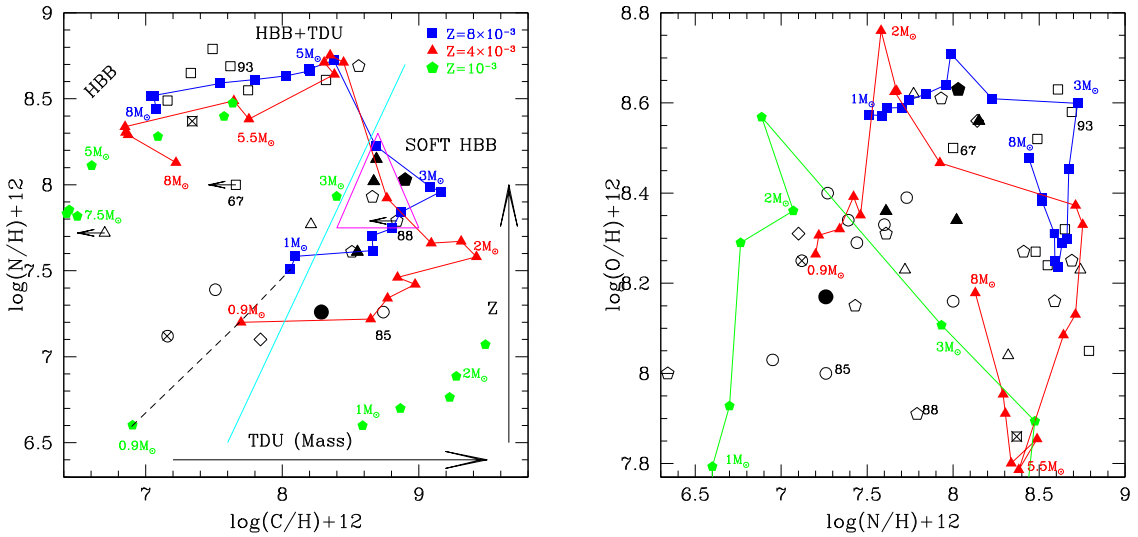


**Figure 4.** Left: stellar evolutionary models and PN data in the nitrogen versus carbon abundance plane. Carbon and nitrogen abundances of LMC PNe symbols are, according to their morphology, squares: bipolar; triangles: bipolar core; circles: round; pentagons: elliptical; diamonds: undetermined or uncertain morphology. The data symbols are filled where carbon dust, crossed where oxygen dust, has been detected. The loci of the AGB model final mass fractions are indicated with filled squares, triangles, and pentagons for $Z = 8 \times 10^{-3}$, $Z = 4 \times 10^{-3}$, and $Z = 10^{-3}$, respectively. Models of different initial mass and the same metallicity are connected with solid lines; for clarity reasons, $Z = 10^{-3}$ models are not joined with any line. For the metallicities $Z = 4, 8 \times 10^{-3}$ we show models of mass in the range $1\,M_{\odot} \leq M \leq 8\,M_{\odot}$, with steps of $0.25\,M_{\odot}$ and $0.5\,M_{\odot}$ in the intervals, respectively, $1\,M_{\odot} \leq M \leq 2\,M_{\odot}$ and $2\,M_{\odot} \leq M \leq 8\,M_{\odot}$. In the $Z = 10^{-3}$ case the overall mass interval is $1\,M_{\odot} \leq M \leq 7.5\,M_{\odot}$, with steps of $0.25\,M_{\odot}$ in the low-mass regime ($1\,M_{\odot} \leq M \leq 1.5\,M_{\odot}$) and $0.5\,M_{\odot}$ for masses above $2\,M_{\odot}$. $0.9\,M_{\odot}$ models are also indicated for $Z = 1, 4 \times 10^{-3}$. For some models the initial mass of the precursor is indicated. The dashed line indicates the locus of expected C and N abundances after the first dredge-up. The solid, diagonal (cyan) line separates the C-rich (right) from the O-rich (left) region. The triangular (magenta) region delimits the region populated by stars near the threshold mass to ignite HBB (see text for details). The horizontal large arrow indicates the in the low-mass regime the stars of higher mass accumulate more carbon at the surface, owing to the higher number of TDU episodes experienced; the vertical large arrow indicates that the surface nitrogen content of low-mass AGBs increases with the metallicity of the star. Right: same plot, but in the oxygen versus nitrogen abundance plane. Symbols are as in the left-hand panel. In both plots, numbers indicate individual LMC PNe as in Table 1.

final mass fractions of carbon and nitrogen, derived from the evolutionary models, have been plotted on the same scale. In this plot the observed PNe are indicated with different symbols, depending on both their morphology and dust types. The model symbols have different colours and shapes depending on their metallicity.

The correlation of PN properties with progenitor mass is analysed on the basis of the stellar evolution processes seen in the previous section. For a given metallicity, the chemistry of the lowest masses shown ($M \sim 1\,M_{\odot}$) reflects essentially the effects of the first dredge-up, with a reduction of the initial carbon and the increase in the surface nitrogen. Stars of higher mass (still below HBB activation) experience more TDU events, thus their final chemistry will be richer in carbon, whereas nitrogen keeps approximately constant.

For masses $M \sim 2.5\,M_{\odot}$ the theoretical sequences bend leftwards. Models of mass around the threshold limit to activate HBB (see discussion in Section 3.3) experience soft HBB, with a slight enhancement of the surface N, and partial destruction of the carbon previously accumulated. These models are included in the triangular region in the figure.

For $M > 3.5\,M_{\odot}$, the final nitrogen is greatly increased by HBB. In agreement with the arguments discussed in Section 3.2, the most massive models occupy the upper-left side of the plane, as their surface chemical composition is not contaminated by TDU, which favours very small carbon abundances. Models of lower mass end their AGB evolution with a higher surface carbon, owing to the effects of a few TDU episodes in the final stages, when HBB is extinguished.

In the CN plane the metallicity effect is more clearly seen in the low-mass regime, as these models evolve at approximately constant N, thus their position is sensitive to the initial chemical composition, particularly the original nitrogen when the star formed. In the high-mass domain the differences among the various metallicities are much smaller, because the C versus N trend mainly reflects the equilibria of CN cycling.

As shown in Fig. 4, the models encompass observed groups of PNe. In particular, we note the dichotomy in the distribution of stars, divided into nitrogen-rich ($\log(N/H) + 12 > 8.3$) and nitrogen-poor ($\log(N/H) + 12 < 8.2$) groups.

### 4.3 Nitrogen-rich PNe

By comparing the AGB final chemical composition to the observed LMC PN abundances we interpret that N-rich PNe, most of which exhibit a bipolar morphology, are the progeny of stars with initial mass above $\sim 4\,M_{\odot}$ that have experienced HBB during their AGB evolution. The most carbon-poor PNe in the LMC ($\log(C/H) + 12 < 7.5$) belong to this group and are the descendants of the most massive AGB stars, whose surface chemical composition reflects the effects of pure HBB. Conversely, PNe with a higher carbon (but that are still N-rich) correspond to the final phase of the evolution of smaller mass progenitors, whose surface chemistry was contaminated by both HBB and TDU.

Given the evolutionary time-scales of AGB stars within this range of mass, we conclude that this PN subsample has progenitors of mass above $\sim 4\,M_{\odot}$, younger than $\sim 200$ Myr. In particular, the nitrogen-rich and carbon-poor PNe have ages $\sim 40$–$80$ Myr and descend from stars of mass in the range $6\,M_{\odot} < M < 8\,M_{\odot}$.

The analysis of the position of the N-rich sample in the CN plane does not allow us to draw information on the PN progenitor's metallicity since the final chemistry of stars experiencing HBB is fairly

independent of the original chemical composition. As shown in the left-hand panel of Fig. 4, models of different metallicity overlap with the observations. The NO plane is more useful to this aim, because the final oxygen abundance is extremely sensitive to the initial metallicity. In the right-hand panel of Fig. 4, we note that most of LMC PNe with enhanced nitrogen can be favourably compared with $Z = 8 \times 10^{-3}$ models of mass in the range $4\,M_{\odot} \leq M \leq 8\,M_{\odot}$, with the exception of SMP21, an N-rich ($\log(N/H) + 12 \sim 8.4$) PN surrounded by oxygen-rich dust. The low (gas) oxygen content of this PN ($\log(O/H) + 12 \sim 7.85$) seems to indicate a low metallicity ($Z = 4 \times 10^{-3}$) precursor with initial mass ∼6–7 $M_{\odot}$. This interpretation is further confirmed by the Ar content of the PN (Leisy & Dennefeld 2006), which is the lowest among the N-rich PNe observed.

### 4.4 The progeny of low-mass AGB stars

The sample of LMC PNe shown in the CN plane includes PNe with $\log(N/H) + 12 < 7.7$, mostly with round or elliptical morphology. According to the comparison with our models, these are the descendants of stars with mass below ∼2.5 $M_{\odot}$. The spread in the observed nitrogen is an effect of a difference in the progenitor metallicity, higher-$Z$ stars having higher nitrogen mass fraction. The observed spread in carbon is an indication of how many TDU episodes the progenitor star experienced during the AGB evolution; according to the discussion in Section 3.1, models of higher mass experience more TDU episodes so that they end their evolution with a higher content of carbon. The trend in carbon is, in this case, a trend in mass. Both the effects of mass and metallicity are indicated, respectively, with a horizontal and a vertical, large arrow in the left-hand panel of Fig. 4.

PNe belonging to this low-carbon subsample are the descendants of stars of mass ∼1 $M_{\odot}$, showing contamination from the first dredge-up only. The age of their progenitor stars is in the range of 5–10 Gyr. In the CN plane, they are close to the dashed line.

Other carbon-rich PNe compare well with higher mass model (∼1.5–2.5 $M_{\odot}$) yields and with progenitors formed between ∼500 Myr and ∼2 Gyr ago.

An additional group of LMC PNe show both carbon and nitrogen enhancement. They are enclosed within the triangular region in the left-hand panel of Fig. 4. We interpret these as the progeny of stars with mass close to the threshold value to activate HBB ($M \sim 3\,M_{\odot}$) discussed in Section 3.3. The enhancement in nitrogen is due to weak HBB experienced in the AGB phases prior to the C-star stage, after which the stars have undergone a series of TDU episodes that increased the surface carbon.

### 4.5 A few outliers

The comparison among the observed abundances and the surface chemical composition in the final evolutionary phases allows an interpretation of most LMC PNe whose CNO abundances are known in terms of the mass (i.e. age) and metallicity of the progenitors.

None the less, there are a few outliers. Four PNe apparently fall outside the range of CNO abundances covered by the models and thus deserve dedicated analysis. These PNe, indicated in the CN plane with the corresponding SMP numbers, are SMP 67, SMP 85, SMP 88, and SMP 93.

(i) SMP 67: the position of this PN in the CN plane is apparently not encompassed by any model. However, the carbon abundance observed for SMP 67 is an upper limit, based on non-detection (see Leisy & Dennefeld 2006 for details), opening the possibility that this is the descendant of a massive AGB stars that experienced HBB with little (or no) contamination from TDU. The bipolar morphology also points to this interpretation. The oxygen content, as shown in the right-hand panel of Fig. 4, is compatible with the $Z = 8 \times 10^{-3}$ metallicity.

(ii) SMP 85: from the position in the CN plane (see left-hand panel of Fig. 4), this round-shaped PN could be the descendent of a low-mass star of $Z = 4 \times 10^{-3}$ that experienced some carbon enrichment, owing to the effects of a few TDUs. The observed low oxygen abundance is hard to compare with any of the models.

(iii) SMP 88: the main problem in the interpretation of the chemistry of this PN is its low oxygen content, which rules out the possibility that it is the descendant of a low-mass star of metallicity $Z = 4$–$8 \times 10^{-3}$, as deduced from its position in the CN plane. Taking into account that carbon was not detected for this object (an upper limit in given based on the spectrum), and considering a typical error on the oxygen content of ∼0.1 dex, we suggest that this PN originates from a low-metallicity star of mass ∼3 $M_{\odot}$, falling in the sample of AGB stars undergoing modest HBB and then becoming carbon star. This hypothesis is confirmed by the very small Ar content ($\log(Ar/H) + 12 = 5.61$).

(iv) SMP 93: in the CN plane, this bipolar PN is compatible with being the product of evolution from an AGB star that underwent HBB and (possibly) of some TDU processing. The problem in the interpretation of this object is its position in the NO plane, where the high oxygen abundance is compatible with a low-mass progenitor, a progenitor that experienced soft HBB and several TDU episodes. If the oxygen abundance observed is overestimated by ∼0.2 dex, the chemistry of the star would be then compatible with its being the descendant of a massive AGB of metallicity $Z = 4 \times 10^{-3}$.

## 5 PNe IN THE LMC AS PROBES OF STELLAR EVOLUTION THEORY

The dichotomy in the distribution of PNe in the CN plane, particularly the division among N-rich ($\log(N/H) + 12 > 8.3$) and N-poor objects, confirms the existence of a threshold in mass, above which the stars experience HBB and become enriched in nitrogen. In the present analysis, we find that HBB is active in all stars of initial mass above ∼3 $M_{\odot}$. This limit is partly dependent on convection modelling and on the assumptions concerning the overshoot from the convective core during the core H-burning phase; other research groups find a slightly higher threshold mass (∼4 $M_{\odot}$) at the same metallicities discussed here (Karakas 2010).

The existence of a group of nitrogen-rich and carbon-poor PNe indicates that the surface chemistry of their precursors have been contaminated mainly by HBB. These stars exhibit a pure HBB chemistry and, according to our interpretation, they descend from very massive ($M > 6\,M_{\odot}$) AGB stars, undergoing a small number of weak thermal pulses. While some effects of TDU during the AGB evolution cannot be disregarded, the observed, small abundances of carbon rule out the possibility that any TDU episode occurred in the very final AGB phases, when HBB was no longer active: indeed, this would determine an increase in the carbon mass fraction.

This finding offers an important opportunity to discriminate among the models of massive AGB stars present in the literature. The dissimilarities among the results presented by various research groups is an indication of the uncertainties affecting the modelling of these stars, mainly owing to the extreme sensitivity of the results obtained concerning the description of convection and mass-loss

(Ventura & D'Antona 2011; Ventura et al. 2013; Doherty et al. 2014b). Doherty et al. (2014a) outlined the relevant effect of the treatment of the convective boundaries on the possible occurrence of TDU in massive AGBs and concluded that the differences among the carbon yields between their models and those presented by Siess (2010, see fig. 15 in Doherty et al. 2014a) were due to the different methods used to determine the extent of the mixed region at the base of the convective mantle. The presence of PNe with very small carbon contents is an indication that the chemistry of massive AGBs is not (or only scarcely) contaminated by TDU, in agreement with Siess (2010) and Ventura & D'Antona (2011).

All nitrogen-rich PNe studied here have C/O < 1. Understanding whether this result is limited to the sample of PNe studied here, or whether it can be generalized to all the PNe in the LMC, would be crucial to assessing the variation of the surface chemical composition of AGBs with mass 4–6 $M_{\odot}$, that experience soft HBB, with temperatures below ∼80 MK. Frost et al. (1998) suggested that these stars would eventually reach the C-star stage as a consequence of a series of TDU episodes after HBB was shut down by the loss of the external mantle. The results of Karakas (2010), based on full evolutionary computations, confirmed this possibility. Conversely, results presented by Ventura et al. (2013) indicate that the C-star stage is never reached by models experiencing HBB, which leaves no room for the possibility of observing PNe enriched in nitrogen and with C/O above unity. The observation of some PNe in the upper region of the CN plane, on the right of the line separating oxygen-rich objects from carbon-rich PNe (see left-hand panel of Fig. 4), would confirm the mechanism suggested by Frost et al. (1998) for forming bright carbon stars.

Still in the context of models experiencing HBB, we note that while the chemical composition in the final evolutionary phases of massive AGB stars of metallicity $Z = 4,\ 8 \times 10^{-3}$ are in good agreement with the observed PN abundances of C, N, and O, the same does not hold for the low-$Z$ component. The reason is that these stars, within the present modelling of convection based on the FST treatment, are expected to experience strong HBB (Ventura & D'Antona 2005), with a considerable depletion of the surface oxygen (see right-hand panel of Fig. 1); this is at odds with other models in the literature (Karakas 2010), where the oxygen destruction (if any) is scarce. The right-hand panel of Fig. 4 shows that such extremely low abundances of oxygen are indeed not found in the present sample of PNe. A possible explanation for this is an observational bias towards the PNe with high oxygen, which is possible by having selected PNe that are λ5007-bright and thus, at low metallicity, typically oxygen-rich (Stanghellini et al. 2003). Alternatively, the HBB produced by low-metallicity, massive AGB models, where convection is treated within the FST framework, is overestimated.

The detection of carbon-enriched PNe that are partly nitrogen-enriched confirms the mechanism of quenching of HBB, favoured by the achievement of the C-star stage. The presence of these PNe further supports the necessity of using the low-temperature, carbon-rich opacities when modelling these evolutionary phases, as pointed out by Marigo (2002, 2007).

Following the discussion in Section 4.4, the PNe on the lower-right side of the CN plane are interpreted as the progeny of stars with initial mass below the threshold needed to activate HBB. The observations indicate an upper limit to the carbon abundance ($\log(C/H) + 12 < 9$), which corresponds to a surface mass fraction $X(C) \sim 10^{-2}$. This is in agreement with our predictions, with the exception of models of mass ∼2–2.5 $M_{\odot}$, that reach slightly higher surface carbon in the late evolutionary AGB phases.

In low-mass AGBs, the final surface carbon is the outcome of a series of TDU events that gradually enrich the external mantle in carbon. The result depends on a delicate interplay between the rate at which mass is lost and the extent of TDU: the former determines the number of thermal pulses (and hence of TDU episodes) experienced by the stars during the AGB phase, whereas a more efficient TDU favours a faster increase in the surface carbon. The upper limit given above, if confirmed, indicates that once the C-star stage is reached, the external mantle is lost rapidly, thus limiting the number of thermal pulses experienced; radiation pressure acting on solid carbon dust particles could be a possible explanation for the increase in the mass-loss rate during these phases. This is in agreement with the AGB models used in the present investigations and with other models in the literature predicting only a modest increase in the surface carbon, with a final C/O ratio below ∼4 (Weiss & Ferguson 2009).

On the other hand, AGB models by other groups predict much higher carbon enrichments, with C/O ratios up to C/O ∼ 10 (Karakas & Lattanzio 2007; Cristallo et al. 2011). The results obtained here would suggest that the extent of the TDU experienced by carbon stars is lower than predicted by the latter models and/or that mass is lost much faster from the external envelope. To discriminate among the various models further observations of C-rich PNe in the LMC are required.

## 6 CONCLUSIONS

We analysed the LMC PNe whose direct CNO abundances are available from space- and ground-based observations, and compared them with the chemical composition of stars of mass $1\,M_{\odot} < M < 8\,M_{\odot}$ based on AGB evolution, accounting also for dust formation in the circumstellar envelope.

The observed abundances of carbon, nitrogen, and oxygen of the PNe sample encompass the final surface chemical composition of the AGB models that we used for the comparison, which allows us to characterize the PNe sample in terms of age, chemical composition, and mass of the progenitors.

The chemical composition of the PNe exhibits a dichotomy in the distribution of the nitrogen abundances, which we interpret as due to the activation of HBB in the stars of initial mass above ∼3 $M_{\odot}$. The objects enriched in nitrogen, with $\log(N/H) + 12 > 8$, are the progeny of stars with mass higher than the aforementioned threshold, formed 50–200 Myr ago. The spread in the carbon content of these nitrogen-rich PNe is explained by the different number of TDU episodes experienced, particularly in the very late evolutionary phases, when HBB is shut down by the envelope consumption.

The N-rich PNe with the lowest carbon abundance are interpreted as the progeny of massive AGB stars with $M \geq 6\,M_{\odot}$, whose surface chemistry reflects mainly the effects of HBB, with a modest contamination from TDU. The very low carbon abundances of these stars confirms that efficient HBB occurs at the base of the envelope of massive AGB stars, in agreement with the predictions of the FST modelling of convection. The lack of carbon stars among the N-rich group suggests that formation of bright C-stars via repeated TDU episodes following HBB quenching does not occur: this is in agreement with our modelling, though additional measurements of carbon abundances of LMC PNe are required to clarify this issue further.

PNe with $\log(N/H) + 12 < 7.5$ are interpreted as the final stages of stars that did not experience any HBB. These objects, with initial mass below ∼3 $M_{\odot}$, formed between 500 Myr and 10 Gyr ago. Whereas the spread in the carbon measured originates from the

different number of TDU episodes experienced, the variation in the nitrogen content reflects the difference in the metallicity.

The highest carbon abundances found in the present sample of PNe suggests an upper limit to the amount of carbon accumulated at the surface of these stars, with $\log(C/H) + 12 < 9$. This finding, if confirmed, indicates that once the C-star phase is reached, the stars lose their external mantle very rapidly, thus limiting the number of further TDU episodes experienced. Other observations are needed to confirm this conclusion.

## ACKNOWLEDGEMENTS

We are particularly indebted to the anonymous referee for the careful reading of the manuscript, that helped improving the quality of the paper. PV was supported by PRIN MIUR 2011 'The Chemical and Dynamical Evolution of the Milky Way and Local Group Galaxies' (PI: F. Matteucci), prot. 2010LY5N2T. DAGH acknowledges support provided by the Spanish Ministry of Economy and Competitiveness under grant AYA-2011-27754 and AYA2014-58082-P. MDC acknowledges support from the Observatory of Rome.

## REFERENCES

Blöcker T., 1995, A&A, 297, 727
Blöcker T., Schöenberner D., 1991, A&A, 244, L43
Canuto V. M. C., Mazzitelli I., 1991, ApJ, 370, 295
Carrera R., Gallart C., Hardy E., Aparicio A., Zinn R., 2008, AJ, 135, 836
Cristallo S. et al., 2011, ApJS, 197, 17
Dell'Agli F., Ventura P., García-Hernández D. A., Schneider R., Di Criscienzo M., Brocato E., D'Antona F., Rossi C., 2014, MNRAS, 442, L38
Dell'Agli F., Ventura P., Schneider R., Di Criscienzo M., García-Hernández D. A., Rossi C., Brocato E., 2015, MNRAS, 447, 2992
Di Criscienzo M. et al., 2013, MNRAS, 433, 313
Doherty C. L., Gil-Pons P., Lau H. H. B., Lattanzio J. C., Siess L., 2014a, MNRAS, 437, 195
Doherty C. L., Gil-Pons P., Lau H. H. B., Lattanzio J. C., Siess L., Campbell S. W., 2014b, MNRAS, 441, 582
Epchtein N. et al., 1994, Ap&SS, 217, 3
Feast M., 1999, PASP, 111, 775
Ferrarotti A. D., Gail H. P., 2006, A&A, 553, 576
Frost C. A., Cannon R. C., Lattanzio J. C., Wood P. R., Forestini M., 1998, A&A, 332, L17
García-Hernández D. A., García-Lario P., Plez B., D'Antona F., Manchado A., Trigo-Rodrguez J. M., 2006, Science, 314, 1751
García-Hernández D. A., García-Lario P., Plez B., Manchado A., D'Antona F., Lub J., Habing H., 2007a, A&A, 462, 711
García-Hernández D. A., Perea-Calderón J. V., Bobrowsky M., García-Lario P., 2007b, ApJ, 666, L33
García-Hernández D. A. et al., 2009, ApJ, 705, L31
Groenewegen M. A. T., de Jong T., 1993, A&A, 267, 410
Harris J., Zaritsky D., 2009, ApJ, 138, 1243
Herwig F., 2005, ARA&A, 43, 435
Izzard R. G., Tout C. A., Karakas A. I., Pols O. R., 2004, MNRAS, 350, 407
Karakas A. I., 2010, MNRAS, 403, 1413
Karakas A. I., 2011, in Kerschbaum F., Lebzelter T., Wing R. F., eds, ASP Conf. Ser. Vol. 445, Why Galaxies Care about AGB Stars II: Shining Examples and Common Inhabitants. Astron. Soc. Pac., San Francisco, p. 3
Karakas A., Lattanzio J. C., 2007, PASA, 24, 103
Karakas A. I., Lattanzio J. C., 2014, PASA, 31, e030
Kingsburgh R. L., Barlow M. J., 1994, MNRAS, 271, 257
Leisy P., Dennefeld M., 2006, A&A, 456, 451
McSaveney J. A., Wood P. R., Scholz M., Lattanzio J. C., Hinkle K. H., 2007, MNRAS, 378, 1089
Marigo P., 2002, A&A, 387, 507
Marigo P., 2007, A&A, 467, 1139
Marigo P., Aringer B., 2009, A&A, 508, 1538
Marigo P., Girardi L., Bressan A., 1999, A&A, 344, 123
Marigo P., Girardi L., Chiosi C., 2003a, A&A, 403, 225
Marigo P., Bernard-Salas J., Pottasch S. R., Tielens A. G. G. M., Wesselius P. R., 2003b, A&A, 409, 619
Marigo P., Bressan A., Girardi L., Aringer B., Gullieuszik M., Groenewegen M. A. T., 2011, in Kerschbaum F., Lebzelter T., Wing R. F., eds, ASP Conf. Ser. Vol. 445, Why Galaxies Care about AGB Stars II: Shining Examples and Common Inhabitants. Astron. Soc. Pac., San Francisco, p. 431
Mazzitelli I., 1989, ApJ, 340, 249
Meixner M. et al., 2006, AJ, 132, 2268
Meixner M. et al., 2010, A&A, 518, L71
Meixner M. et al., 2013, ApJ, 146, 62
Nanni A., Bressan A., Marigo P., Girardi L., 2013a, MNRAS, 434, 488
Nanni A., Bressan A., Marigo P., Girardi L., 2013b, MNRAS, 434, 2390
Nanni A., Bressan A., Marigo P., Girardi L., 2014, MNRAS, 438, 2328
Piatti A. E., Geisler G., 2013, AJ, 145, 17
Renzini A., Voli M., 1981, A&A, 94, 175
Schlegel D. J., Finkbeiner D. P., Davis M., 1998, ApJ, 500, 525
Schneider R., Valiante R., Ventura P., Dell'Agli F., Di Criscienzo M., Hirashita H., Kemper F., 2014, MNRAS, 442, 1440
Shaw R. A., Stanghellini L., Mutchler M., Balick B., Blades J. C., 2001, ApJ, 548, 727
Shaw R. A., Stanghellini L., Villaver E., Mutchler M., 2006, ApJS, 167, 201
Siess L., 2010, A&A, 512, A10
Skrutskie M. F. et al., 2006, AJ, 131, 1163
Stanghellini L., Shaw R. A., Balick B., Blades J. C., 2000, ApJ, 534, L167
Stanghellini L., Shaw R. A., Balick B., Mutchler M., Blades J. C., Villaver E., 2003, ApJ, 596, 997
Stanghellini L., Shaw R. A., Gilmore D., 2005, ApJ, 622, 294
Stanghellini L., Garcia-Lario P., García-Hernández D. A., Perea-Calderón J. V., Davies J. E., Manchado A., Villaver E., Shaw R. A., 2007, ApJ, 671, 1669
Stanghellini L., Lee T.-H., Shaw R. A., Balick B., Villaver E., 2009, ApJ, 702, 733
Ventura P., D'Antona F., 2005, A&A, 431, 279
Ventura P., D'Antona F., 2009, MNRAS, 499, 835
Ventura P., D'Antona F., 2011, MNRAS, 410, 2760
Ventura P., Marigo P., 2009, MNRAS, 399, L54
Ventura P., Marigo P., 2010, MNRAS, 408, 2476
Ventura P., Zeppieri A., Mazzitelli I., D'Antona F., 1998, A&A, 334, 953
Ventura P. et al., 2012a, MNRAS, 420, 1442
Ventura P. et al., 2012b, MNRAS, 424, 2345
Ventura P., Di Criscienzo M., Carini R., D'Antona F., 2013, MNRAS, 431, 3642
Ventura P., Di Criscienzo M. D., D'Antona F., Vesperini E., Tailo M., Dell'Agli F., D'Ercole A., 2014a, MNRAS, 437, 3274
Ventura P., Dell'Agli F., Di Criscienzo M., Schneider R., Rossi C., La Franca F., Gallerani S., Valiante R., 2014b, MNRAS, 439, 977
Ventura P., Karakas A. I., Dell'Agli F., Boyer M. L., García-Hernández D. A., Di Criscienzo M., Schneider R., 2015, MNRAS, 450, 3181
Wachter A., Schröder K. P., Winters J. M., Arndt T. U., Sedlmayr E., 2002, A&A, 384, 452
Wachter A., Winters J. M., Schröder K. P., Sedlmayr E., 2008, A&A, 486, 497
Weiss A., Ferguson J. W., 2009, A&A, 508, 1343
Weisz D. R., Dolphin A. E., Skillman E. D., Holtzman J., Dalcanton J. J., Cole A. A., Neary K., 2013, MNRAS, 431, 364
Zamora O., García-Hernández D. A., Plez B., Manchado A., 2014, A&A, 564, L4
Zaritsky D., Harris J., Thompson I. B., Grebel E. K., 2004, AJ, 128, 1606
Zhukovska S., Henning T., 2013, A&A, 555, 99

This paper has been typeset from a TEX/LATEX file prepared by the author.